Copper Can Still Be Epitaxially Deposited on Palladium Nanocrystals To Generate Core–Shell Nanocubes Despite Their Large Lattice Mismatch

Mingshang Jin,[†,‡] Hui Zhang,[†,§] Jinguo Wang,[⊥] Xiaolan Zhong,[¶] Ning Lu,[⊥] Zhiyuan Li,[¶] Zhaoxiong Xie,[‡] Moon J. Kim,[⊥,#] and Younan Xia[†,▽,*]

[†]Department of Biomedical Engineering, Washington University, St. Louis, Missouri 63130, United States, [‡]State Key Laboratory for Physical Chemistry of Solid Surfaces and Department of Chemistry, Xiamen University, Xiamen, Fujian 361005, People's Republic of China, [§]State Key Laboratory of Silicon Materials and Department of Materials Science and Engineering, Zhejiang University, Hangzhou, Zhejiang 310027, People's Republic of China, [⊥]Department of Materials Science, University of Texas at Dallas, Richardson, Texas 75083, United States, [¶]Institute of Physics, Chinese Academy of Sciences, Beijing 100190, People's Republic of China, and [#]Department of Nanobio Materials and Electronics, World Class University, Gwangju Institute of Science and Technology, Gwangju 500-712, Korea. [▽]Present address: Georgia Institute of Technology, Atlanta, Georgia 303322.

ABSTRACT Here we report the synthesis of Pd@Cu core–shell nanocubes *via* epitaxial growth, where the lattice mismatch is 7.1%. The synthesis involved the use of Pd seeds with different shapes (including cubes, cuboctahedra, and octahedra) for the epitaxial growth of Cu shells. Different from the conventional growth mode, Cu atoms initially nucleated only on a few of the many faces of a Pd seed, onto which more Cu atoms were continuously added to generate Cu blocks. Later, the Cu atoms also started to nucleate and grow on other faces of the Pd seed until the entire surface of the seed was covered by a Cu shell. As a result, the Pd seed was rarely located in the center of each core–shell structure. The final product took a cubic shape enclosed by {100} facets regardless of the type of Pd seeds used because of the selective capping of Cu(100) surface by hexadecylamine. The edge lengths of the Pd@Cu nanocubes could be tuned from 50 to 100 nm by varying the amount of Pd seeds while keeping the amount of $CuCl_2$ precursor.

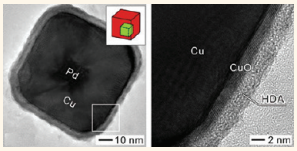

KEYWORDS: core–shell structure · lattice mismatch · epitaxial growth

Bimetallic core–shell nanocrystals are of great importance for a range of applications in catalysis, plasmonics, and surface-enhanced Raman spectroscopy (SERS).[1−5] The nanocrystal is commonly prepared *via* conformal deposition of a shell on the surface of a seed made of a different metal.[6−12] In general, both epitaxial and nonepitaxial growth can occur depending on the degree of lattice mismatch. Typically, epitaxial growth takes place only when the lattice mismatch is below 5%.[13] As a result, single-crystal, bimetallic nanocrystals with a core–shell structure have been mainly reported for pairs of metals such as Au and Ag (lattice mismatch: 0.2%) or Pt and Pd (lattice mismatch: 0.85%). To this end, Yang and co-workers demonstrated the synthesis of single-crystal Pt@Pd core–shell nanocrystals in the shape of cubes, cuboctahedra, and octahedra *via* epitaxial growth of Pd shells on Pt cubic seeds.[14] Tian and co-workers reported the synthesis of single-crystal Au@Ag core–shell nanocubes *via* epitaxial overgrowth of Ag on Au octahedral seeds.[13] Our group also demonstrated the synthesis of single-crystal Au@Ag core–shell nanocubes,[5] and the synthesis of multishelled nanocrystals composed of alternating Pd and Pt shells by starting with seeds made of Pd or Pt nanocrystals.[9] In a series of reports, Tian and co-workers also extended their synthesis to generate Au@Pd core–shell nanocrystals where the lattice mismatch of 4.7% approaches the limit of 5% set by them and other research groups.[13,15,16]

The limitation associated with lattice mismatch has become one of the most significant constraints in generating bimetallic core–shell nanocrystals, particularly for the preparation of core–shell nanocrystals with a single-crystal structure and well-defined shapes. Attempts to use epitaxial growth to produce bimetallic core–shell nanocrystals from two metals with lattice mismatch greater than 5% have been met with limited success so far. For example, the shells are often characterized by a polycrystalline structure, and the final products often take a spherical shape or dendritic morphology due to the lack of an epitaxial relationship

* Address correspondence to younan.xia@bme.gatech.edu.

Received for review December 22, 2011 and accepted February 3, 2012.

Published online February 03, 2012
10.1021/nn2050278

between the core and the shell.[17−19] Recently, a number of groups have started to address this issue. To this end, Tsuji and co-workers demonstrated the syntheses of Au@Cu and Au@Ni core−shell nanoparticles, where the lattice mismatches were 11.4% and 13.6%, respectively.[20,21] Our group also reported a facile method for epitaxial growth of Ag on Pd nanocubes, in which the nucleation and growth of Ag could be controlled on one, three, or six of the equivalent {100} faces of a Pd cubic seed.[22] As a major advancement, these studies demonstrated the ability to generate bimetallic core−shell nanocrystals from two metals with lattice mismatches greater than 5%. However, there was essentially no control over the thickness of the shell and the final shape taken by the product. In addition, the growth mechanism was also unclear.

In this work, we chose the Pd and Cu pair as a model system to investigate the formation of core−shell nanocrystals from two metals with lattice mismatch greater than 5%. We have successfully prepared Pd@Cu core−shell nanocubes *via* the reduction of $CuCl_2$ by glucose in the presence of Pd seeds and hexadecylamine (HDA), a selective capping agent for the {100} facets of Cu.[23] The edge length of the as-obtained Pd@Cu core−shell nanocubes could be easily controlled by varying the proportion of the seed relative to the precursor. Our studies indicate that the formation of Pd@Cu core−shell nanocubes followed a localized epitaxial growth mechanism, by which Cu atoms first nucleated only on a few of the many faces of a Pd seed. At a later point, the newly formed Cu atoms started to nucleate and grow on other faces of the seed until its entire surface was covered by a complete shell of Cu. The Pd@Cu core−shell nanocrystals evolved into a cubic shape due to a strong affinity of HDA for the Cu(100) surface.

RESULTS AND DISCUSSION

For the standard synthesis of Pd@Cu core−shell nanocubes (see Experimental Section for details), we used Pd nanocubes of 18 nm in edge length as the seeds. The Pd nanocubes were prepared using a protocol previously reported by our group, which involved the use of KBr as a capping agent.[24] Figure 1A shows a typical TEM image of the as-prepared nanocubes, with purity approaching 100%. The average edge length of these cubes was 18 ± 4 nm. Some of the nanocubes had a slightly elongated shape but their side faces were still covered by {100} planes. We collectively call all of them "nanocubes" in the present work for the purpose of simplicity.

The as-obtained 18-nm Pd nanocubes could be directly used as seeds for the epitaxial growth of Cu shells without any modification or treatment. We recently discovered that Cu nanowires and nanocubes could be prepared by reducing Cu^{2+} ions with glucose in aqueous solutions in the presence of HDA as a capping agent.[23] Here we extended this reaction to the preparation of Pd@Cu core−shell nanocubes by simply introducing some Pd nanocubes into the solution as the seeds. By separating nucleation and growth into two different tasks, we can achieve a better control over the size and shape of resultant nanocrystals.[25−28] Figure 1B shows SEM image of the as-obtained Pd@Cu core−shell nanocubes synthesized using the standard procedure. All of them were cubic in shape, only with slight truncation at the corners (see Supporting Information). The size of the Pd@Cu core−shell nanocubes could be easily tuned by varying the amount of Pd seeds added with other parameters being kept the same as in the standard procedure. For example, by using 1.5, 1.0, and 0.5 mL of the Pd seeds, the resultant Pd@Cu core−shell nanocubes were 50, 75, and 100 nm, respectively, in edge length (Figure 1B−D). Thanks to their good uniformity in size and shape, some of the core−shell nanocubes also crystallized into two- and three-dimensional lattices on the Si substrates during solvent evaporation. The TEM images in the insets clearly show that there was a Pd seed inside each core−shell nanocube.

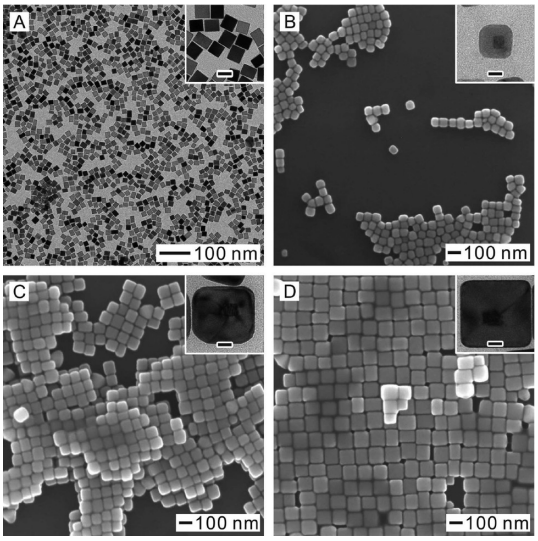

Figure 1. (A) TEM image of 18-nm Pd nanocubes that served as seeds for the deposition of Cu shells, and (B−D) SEM images of Pd@Cu core−shell nanocubes prepared with different volumes of the seed suspension at a concentration of 1.8 mg/mL: 1.5, 1.0, and 0.5 mL. The edge lengths of the core−shell nanocubes were approximately (B) 50, (C) 75, and (D) 100 nm, respectively. The insets show TEM images of the samples, and the scale bars are 20 nm.

We used TEM, high-angle annular dark-field scanning-transmission electron microscopy (HAADF-STEM), high-resolution TEM (HRTEM), and energy dispersive X-ray (EDX) analysis to characterize the morphology, structure, and composition of the 75-nm Pd@Cu core−shell nanocubes prepared using the standard procedure. The Pd seed within the Cu shell could be easily resolved under TEM and HAADF-STEM due to the difference in contrast between Pd and Cu (Figure 2A,B), confirming the formation of a core−shell structure. Interestingly, we found that most of the Pd seeds within the core−shell nanocubes were not located in

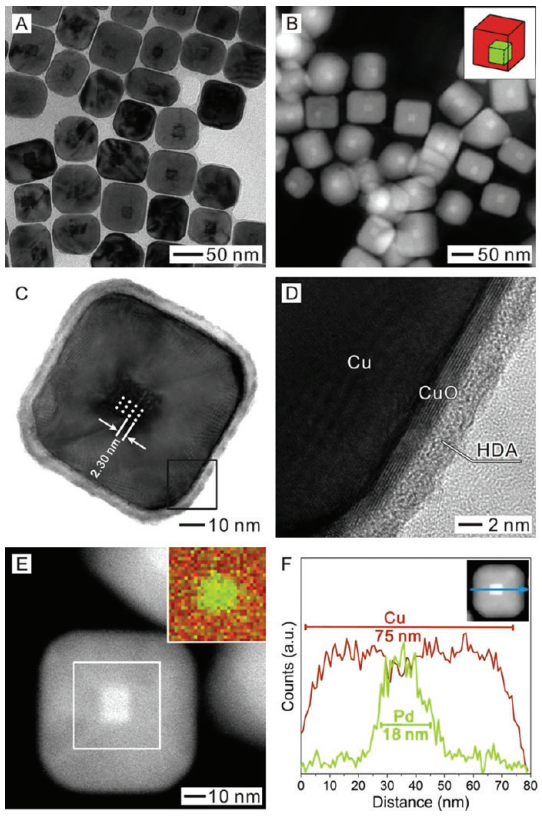

Figure 2. Morphology, structural, and compositional characterizations of the 75-nm Pd@Cu core–shell nanocubes: (A) TEM image, (B) HAADF-STEM image, (C, D) HRTEM image, (E) HAADF-STEM image, and EDX mapping (inset), and (F) line-scan profile. In panel E, the inset was taken from the boxed region, with the green and red colors corresponding to Pd and Cu, respectively.

the center, implying a growth mechanism different from what was often observed during the formation of core–shell nanoparticles. From the TEM and HAADF-STEM images, we could also resolve the orientation of the Pd core relative to the Cu shell. As shown by the model in the inset of Figure 2B, the Pd cube was oriented with one of its side faces parallel to one of the side faces of the Cu shell. Figure 2C shows HRTEM image of an individual Pd@Cu core–shell nanocube viewed along the ⟨001⟩ zone axis. In the Pd region, one can see fringes in the form of alternating bright and dark stripes known as a Moiré pattern. The spacing of the Moiré fringes can be calculated using the following equation: $D = d_1d_2/(d_2 - d_1)$, where D is the spacing between two bright or dark stripes and d_1 and d_2 are the spacing of the two sets of planes involved in the inteference.[29] For the Moiré pattern shown in Figure 2C, the D value was measured as 2.30 nm, in agreement with the value (2.22 nm) calculated from the lattice spacing of {200} planes for both Pd and Cu. The Moiré fringes were parallel to each other in the core area, suggesting that the lattices of Pd and Cu shared the same orientation and there was an epitaxial relationship between the Pd core and the Cu shell.

It is well-known that Cu nanoparticles can be easily oxidized when exposed to air due to the high reactivity of Cu toward oxygen. In comparison, the Pd@Cu core–shell nanocubes prepared using this method were relatively stable because their surfaces were passivated and protected by HDA. As shown in Figure 2D, the Pd@Cu core–shell nanocube was covered by a double layer of HDA about 3 nm in thickness. The existence of a HDA shell may be responsible for the improvement in chemical stability of the Pd@Cu core–shell nanocubes. Previous studies have shown that the amino group of HDA could strongly bind to the surface of Cu and Ag nanocrystals, and thus effectively protect them from oxidation by air.[30,31] Despite the protection by the HDA shell, the Cu atoms on the surface of a Pd@Cu core–shell nanocube could still be oxidized to generate an oxide layer of 1–2 nm in thickness. The HRTEM image in Figure 2D clearly showed two different lattice spacing of 0.18 and 0.25 nm that could be indexed to the (200) planes of Cu and Cu_2O, respectively. The distributions of Pd and Cu in the nanocube were revealed by both EDX mapping and line-scan analysis. The elemental mapping in the inset of Figure 2E clearly shows a major difference in composition between the core (Pd, green) and the shell (Cu, red), confirming a bimetallic, core–shell structure that was also supported by the EDX line-scan data recorded along the middle plane of a single Pd@Cu core–shell nanocube (see Figure 2F and the inset). As expected, both Pd and Cu were detected. The widths of peaks for the Pd and Cu traces matched well the edge lengths of the Pd cubic seed and the Pd@Cu nanocube, respectively.

According to previous studies, the formation of a bimetallic, core–shell nanocrystal *via* epitaxial overgrowth must meet a set of requirments,[13,14] especially the restriction of lattice mismatch. In the case of a lattice mismatch larger than 5%, the overgrowth would result in spherical products with a rough surface or dendritic morphology.[13,14] It is generally accepted that no single-crystal, core–shell nanocrystal could be formed *via* epitaxial growth when the lattice mismatch between the two metals is greater than 5%. In the case of Pd and Cu, their lattice constants are 3.8824 and 3.6077 Å, respectively, corresponding to a lattice mismatch of 7.1%. As such, it is expected epitaxial growth could no longer be used to prepare Pd@Cu core–shell nanocrystals in an aqueous solution.

In an effort to understand why the single-crystal Pd@Cu nanocubes were formed, we took TEM images from a set of products sampled from the same reaction solution at different time points. In the initial stage (Figure 3A, t = 20 min), Cu atoms only nucleated and grew on one or two of the side faces of a Pd nanocube to generate Cu blocks through localized epitaxial growth probably due to a large lattice mismatch between Pd and Cu. This observation is in agreement with the results of previous studies.[14] When the reaction was

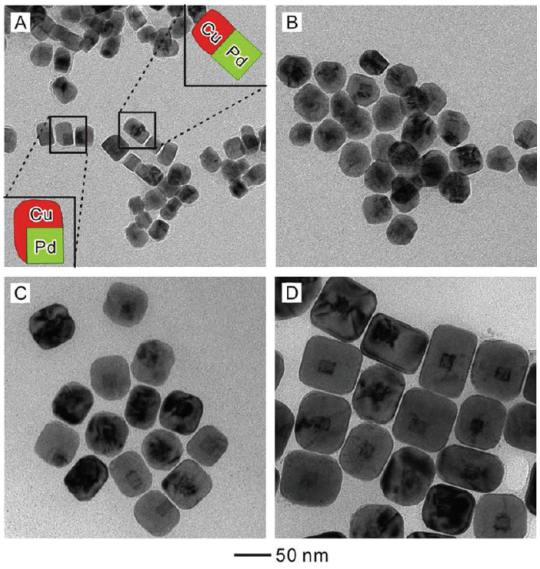

Figure 3. TEM images of intermediates sampled at different stages during the synthesis of 75-nm Pd@Cu core–shell nanocubes: (A) 20, (B) 40, (C) 60, and (D) 180 min.

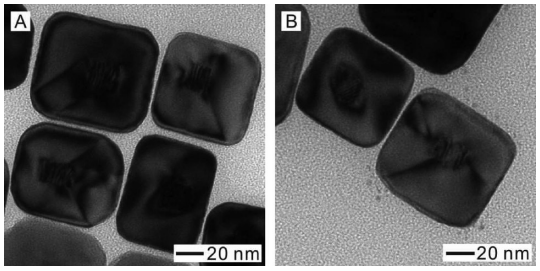

Figure 4. TEM images of the as-obtained 75-nm Pd@Cu nanocubes, clearly showing the existence of darker lines in the shells that emanated from the Pd cores.

extended to t = 40 min (Figure 3B), some of the Pd seeds were completely encased in Cu shells due to the nucleation and growth of Cu on other faces of the Pd seeds. Eventually, all the Pd seeds were encased by Cu shells to generate Pd@Cu core–shell nanocrystals. With the assistance of HDA, the core–shell nanocrystals evolved into a cubic shape with {100} facets expressed on the surface. Taken together, it is clear that the formation of Pd@Cu nanocubes was based on a localized epitaxial growth mechanism. Because different portions of the Cu shell nucleated and grew on the Pd seed at different stages of the synthesis, they tended to have different thicknesses, and thus most of the Pd seeds were not positioned in the centers of the core–shell nanocubes. In addition, it is worth pointing out that there were dark lines in TEM images of the final Pd@Cu core–shell nanocubes, that emanated from the Pd cores and extended into the Cu shells (Figure 4). These dark lines were likely caused by the strains associated with the coalescence of different Cu domains nucleated and grown from different sites of the same Pd seed.

The final structure and morphology taken by the Pd–Cu nanocrystals also depended on the concentration of Cu precursor added in the solution. Figure S1 in the Supporting Information, shows TEM images of Pd–Cu nanocrystals prepared with the use of $CuCl_2$ precursor at three different concentrations. When the concentration was relatively low (1.0 mg/mL), the amount of added $CuCl_2$ would be just sufficient for nucleation and growth on one or two of the six faces of a Pd seed, resulting in the formation of Pd–Cu dimers (Supporting Information, Figure S1A,B). When we increased the concentration of $CuCl_2$ to 2.1 mg/mL while maintaining the volume at 10 mL, the resultant Cu was enough to form a shell on the entire surface of a Pd seed (Figure S1C,D), leading to the formation of Pd@Cu core–shell nanocubes with a final edge length around 75 nm. Further increasing the concentration of $CuCl_2$ to 4.2 mg/mL merely resulted in Pd@Cu core–shell nanocubes with larger sizes. As shown in Figure S1E,F, the average edge length of the Pd@Cu core–shell nanocubes increased to 120 nm. In the last two cases, it was still found that the Pd seeds were not positioned in the centers of the Pd@Cu core–shell nanocubes, implying the involvement of the same localized epitaxial growth of Cu on Pd seeds at high concentrations of Cu precursor. These results indicate that the concentration of Cu precursor may not affect the nucleation and growth mode of Cu on Pd cubic seeds, only leading to the formation of Pd–Cu dimers and Pd@Cu core–shell nanocubes with different sizes. On the basis of the above results, we can conclude that localized epitaxial growth can still lead to the formation of bimetallic, core–shell nanocrystals with a single-crystal structure. This new mechanism also demonstrates the possibility of generating core–shell nanocrystals from two metals with a lattice mismatch larger than 5%, and can thus be used to prepare bimetallic core–shell nanocrystals from a broader range of metals than previously thought.

We further confirmed the epitaxial relationship for the bimetallic core–shell nanocubes by X-ray diffraction (XRD). Figure 5A shows a typical XRD pattern recorded from the 75-nm Pd@Cu nanocubes. Since the nanocubes tended to be oriented with their {100} planes parallel to the substrate, the (200) diffraction peak was stronger in intensity than the (111) diffraction peak. There were two separate phases corresponding to the Pd cores and Cu shells. Significantly, the preferential orientation of the Pd seeds was the same as that of the Cu shells, indicating an epitaxial relationship between these two components. The XRD pattern (Figure 5B) of the Pd@Cu core–shell nanocubes grown from Pd octahedral seeds also showed a preferential orientation for the {100} planes, which is the same as the nanocubes grown from the cubic seeds.

Similar to Ag and Au, Cu is also known to exhibit localized surface plasmon resonance (LSPR) peaks in

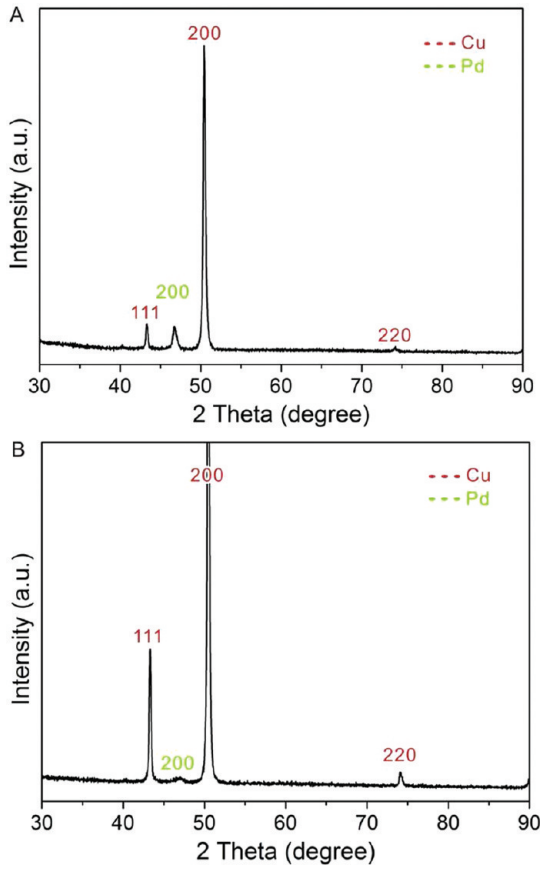

Figure 5. Powder X-ray diffraction patterns of the Pd@Cu core–shell nanocubes with Pd nanocubes (A) and octahedra (B) serving as the seeds.

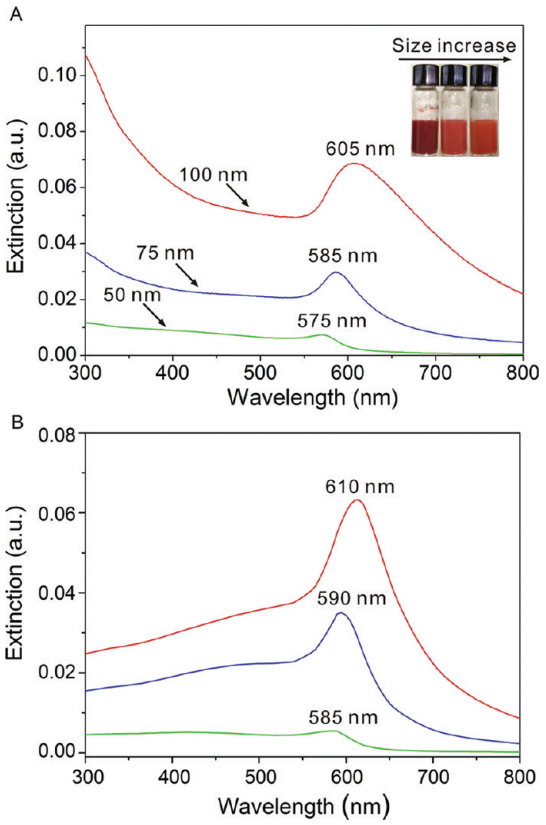

Figure 6. (A) UV–vis spectra recorded from the Pd@Cu nanocubes of different sizes. All samples were suspended in water. The inset in panel A shows a photograph of the as-prepared sample of Pd@Cu core–shell nanocubes. (B) Extinction spectra theoretically calculated for the Pd@Cu core–shell nanocubes with different edge lengths (the nanocubes were surrounded by water too).

the visible region and thus may find use in plasmonics, surface-enhanced Raman scattering (SERS), and other related applications.[32] Here we investigated the LSPR properties of the Pd@Cu core–shell nanocubes with different sizes. Figure 6A shows the extinction spectra recorded from aqueous suspensions of the Pd@Cu core–shell nanocubes with different sizes. When the edge length was increased from 50 to 100 nm, the LSPR peak was red-shifted from 575 to 605 nm. Accordingly, the colors of aqueous suspensions of the Pd@Cu nanocubes changed from purple to red (see the inset in Figure 6A). The 100-nm core–shell nanocubes showed a relatively broad LSPR peak, which could be attributed to their large sizes and thus the involvement of quadruple excitation in addition to dipole excitation. By using the discrete dipole approximation (DDA) method, we also calculated the extinction spectra of Pd@Cu nanocubes with different sizes. We assumed that the Pd@Cu nanocubes were slightly truncated at their corners due to the easiness of oxidation for Cu when exposed to air (see Supporting Information for a detailed description of truncation). Figure 6B shows the results from calculations, which were in good agreement with the experimental data. For example, the LSPR peak was red-shifted from 585 to 590 and 610 nm when the size was increased from 50 to 75 and 100 nm, respectively. These observations are also consistent with the calculation results reported by Wang and co-workers,[33] where the LSPR peak of a metal nanostructure was found to red-shift when the electromagnetic field lines were expelled from the metallic part to the dielectric environment. A similar red-shift was also observed for other metals such as Ag, Au, and Pd.[34–37] Both the experimental and computational results indicate that the size could only be used to tune the LSPR peak of Pd@Cu nanocubes over a relatively narrow window.

To elucidate the effect of Pd seeds on the final shapes taken by the core–shell nanocrystals, Pd seeds with different sizes and shapes were also used for the epitaxial growth of Cu. Figure 7 shows SEM images of Pd cuboctahedra and octahedra used as the seeds, and the corresponding Pd@Cu core–shell nanocubes. It is worth noting that Pd@Cu core–shell nanocubes were also obtained in high quality from these two new types of Pd seeds. Careful examination (insets in Figure 7C,D) revealed that the cuboctahedral or octahedral Pd seed in the core–shell nanocube was projected along the ⟨100⟩ direction, which was the same as that of the Cu shell, thus giving hexagonal and square profiles for the

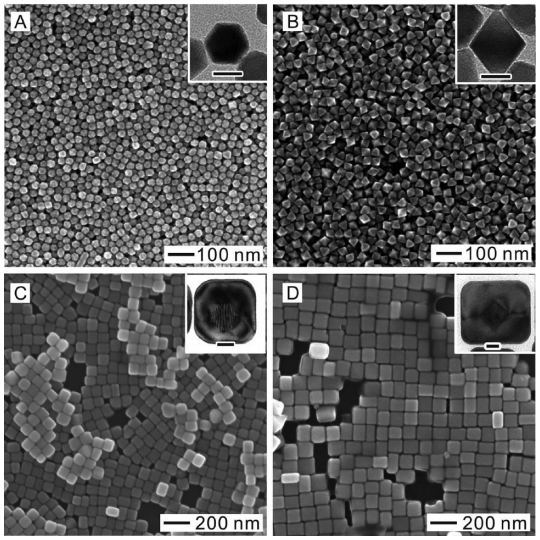

Figure 7. (A,B) SEM images of Pd cuboctahedra and octahedra that served as the seeds for the epitaxial deposition of Cu shells. (C,D) TEM images of the resultant Pd@Cu core–shell nanocubes. The insets show TEM images of individual nanocrystals at higher magnifications. The scale bars in the insets are 20 nm.

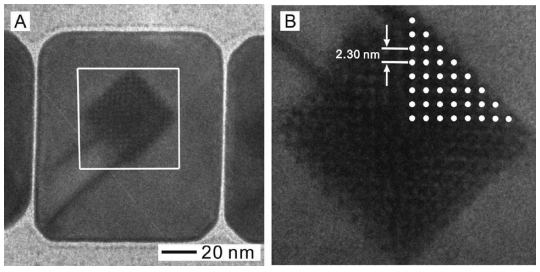

Figure 8. (A) TEM image of a Pd@Cu core–shell nanocube grown from an octahedral seed of Pd. (B) TEM image of the core region as marked by the white box in image A, where the Moiré pattern can be clearly resolved.

cores, respectively. As shown in Figure 8, Moiré patterns similar to that observed in the case of Pd cubic seeds were also observed. The Moiré patterns also confirm that the overgrowth was epitaxial and confined to the ⟨111⟩ directions to give {100} facets on the surface of the Pd@Cu core–shell nanocubes. The Pd seed was also found to be deviated from the center of each core–shell nanocube due to the involvement of a localized epitaxial growth mechanism (Supporting Information, Figure S2). In addition to the effect of shape, we also studied the effect of size for the cubic Pd seeds in this synthesis. In a comparison study, 6-nm Pd cubes were introduced into the reaction as the seeds while other conditions were kept the same as the standard procedure. As shown in Supporting Information, Figure S3, the final product exhibited a cubic core–shell structure similar to those obtained with large Pd cubic seeds. Most of the 6-nm Pd seeds were also deviated from the centers of the Pd@Cu core–shell nanocubes. These experimental data suggest that Cu can be epitaxially deposited on Pd nanocrystals, regardless of the shape and the size for the Pd seeds.

One of the major concerns for core–shell bimetallic nanocrystals is their stability. Many factors can affect the stability of shell made of a second metal. The lattice mismatch should be considered as one of them. In general, bimetallic core–shell nanocrystals with large lattice mismatches should be less stable than those with small lattice mismatches due to the existence of lattice distortions or strains formed during the deposition of shells, and thus higher reactivity. However, in some cases such as Au@Cu, it was found that the core–shell nanoparticles had a higher resistance against oxidation because Au has a much stronger electron drawing effect than that of Cu.[20] In the present system, the Pd@Cu core–shell nanocubes were found to be stable as an aqueous suspension in air, but this stability came from the use of hexadecylamine as the capping agent, which has been proven to be effective in preventing the Cu surface from oxidation in an aqueous medium.

CONCLUSION

We have demonstrated a facile method for epitaxially depositing Cu on Pd nanocrystals to generate Pd@Cu core–shell nanocubes, a process that has been considered to be difficult or impossible due to the large (>5%) mismatch in lattice constant between these two metals. We have also demonstrated the feasibility of tailoring the sizes of the Pd@Cu core–shell nanocubes by simply controlling the ratio of Cu precursor relative to Pd seeds. By paying attention to the intermediate products involved in the formation of Pd@Cu nanocubes, we discovered that the core–shell structure was formed *via* localized epitaxial growth, which is different from the conformal epitaxial growth commonly observed in the synthesis of core–shell nanostructures. The success of our synthesis suggests that all the rules (including the requirement on lattice mismatch between the two metals) that have been proposed for the preparation of bimetallic core–shell structures should be examined again by taking into consideration the nanoscale dimensions for both the core and shell components. With the inclusion of metals bearing a large mismatch in lattice constant into epitaxial growth, we should be able to greatly expand the scope and variation in composition for core–shell nanostructures.

EXPERIMENTAL SECTION

Chemicals and Materials. Sodium tetrachloropalladate (II) (Na_2PdCl_4, 99.998%), copper chloride dihydrate ($CuCl_2 \cdot 2H_2O$), poly(vinyl pyrrolidone) (PVP, MW ≈ 55000), L-ascorbic acid (AA), hexadecylamine ($CH_3(CH_2)_{14}CH_2NH_2$), and glucose ($C_6H_{12}O_6$) were all obtained from Sigma-Aldrich. Potassium bromide

(KBr) and formaldehyde (HCHO) were obtained from Fisher Scientific. Ethanol (200 proof) was obtained from Pharmco Products. The chemical compounds were used as received. All aqueous solutions were prepared using deionized water with a resistivity of 18.2 MΩ·cm.

Synthesis of 18-nm Pd Nanocubes. The Pd nanocubes were synthesized by adding a Na_2PdCl_4 solution into a mixture of AA, KBr, and KCl according to our previous report.[24] In a typical synthesis, 8.0 mL of an aqueous solution containing 105 mg of PVP, 60 mg of AA, and 600 mg of KBr was placed in a vial and preheated to 80 °C in an oil bath under magnetic stirring for 10 min. Subsequently, 3.0 mL of an aqueous solution containing 57 mg of Na_2PdCl_4 was added with a pipet. After the vial had been capped, the reaction was allowed to continue at 80 °C for 3 h. The product was collected by centrifugation, washed three times with water to remove excess PVP, and redispersed in 11 mL of water.

Synthesis of Pd Cuboctahedra and Octahedra. The Pd cuboctahedra and octahedra were synthesized by reducing Na_2PdCl_4 with formaldehyde in an aqueous solution according to our previous report.[38] In a typical synthesis, 3 mL of an aqueous Na_2PdCl_4 solution (32 mM) was introduced into 8 mL of an aqueous solution containing 105 mg PVP, 100 μL HCHO, and 0.3 mL of aqueous suspension (1.8 mg/mL in concentration) of the 18-nm Pd cubic seeds, which had been preheated at 60 °C for 5 min under magnetic stirring in a capped vial. Different from the Ag system, PVP has no selectivity in binding to the Pd(100) and Pd(111) surfaces. As a result, the morphology of resultant Pd polyhedra was determined by the ratio between the amounts of Na_2PdCl_4 (the precursor) and Pd seeds. The addition of Na_2PdCl_4 in the amounts of 8.7 mg and 29.0 mg led to the formation of Pd cuboctahedra and octahedra, respectively. Each reaction was allowed to proceed at 60 °C for 3 h. After collection by centrifugation and washing two times with water, the final product was redispersed in 11 mL of water.

Synthesis of Pd@Cu Core–Shell Nanocubes. The Pd@Cu core–shell nanocubes were prepared using seed-mediated overgrowth. In a standard synthesis, 10 mL of an aqueous solution containing 21 mg of $CuCl_2 \cdot 2H_2O$, 90 mg of hexadecylamine, 50 mg of glucose, and 1.5 mL of the aqueous suspension of Pd seeds (1.8 mg/mL) was placed in a vial. After the vial had been capped, the solution was magnetically stirred at room temperature overnight and then heated to 100 °C in an oil bath for another 3 h. The product was collected by centrifugation, washed three times with ethanol to remove excess PVP, and redispersed in ethanol.

Morphological, Structural, and Elemental Characterizations. Transmission electron microscopy (TEM) images were taken using a Tecnai G2 Spirit Twin microscope (FEI, Hillsboro, OR) operated at 120 kV. High-resolution TEM (HRTEM), high-angle annular dark-field scanning TEM (HAADF-STEM), and energy dispersive X-ray (EDX) analyses were performed using a JEOL 2100F microscope (JEOL, Tokyo, Japan) operated at 200 kV. Scanning electron microscopy (SEM) images were captured using a Nova NanoSEM 230 field-emission microscope (FEI, Hillsboro, OR) operated at 30 kV. Powder XRD patterns were recorded using a diffractometer (DMAX/A, Rigaku) operated at 35 kV and 35 mA. UV–vis spectra were taken with a diode array spectrophotometer (Cary 50, Varian). The concentration of elemental Pd in the suspension of seeds was determined using inductively coupled plasma mass spectrometry (ICP–MS, Perkin-Elmer Elan DRC II).

Conflict of Interest: The authors declare no competing financial interest.

Acknowledgment. This work was supported in part by a DOE subcontract from the University of Delaware (DE-FG02-03 ER15468) and startup funds from Washington University in St. Louis. As a visiting scholar, H.Z. was also partially supported by the "New Star Program" of Zhejiang University. As a visiting Ph. D. student from Xiamen University, M.J. was also partially supported by the China Scholarship Council. M.J.K. was supported by a grant from the World-Class University Program (MEST through NRF, R31-10026).

Supporting Information Available: Definition of the truncation and TEM images of the as-obtained Pd@Cu core–shell nanocubes prepared using conditions different from the standard synthesis. This material is available free of charge *via* the Internet at http://pubs.acs.org.

REFERENCES AND NOTES

1. Yan, J.; Zhang, X.; Akita, T.; Haruta, M.; Xu, Q. One-Step Seeding Growth of Magnetically Recyclable Au@Co Core–Shell Nanoparticles: Highly Efficient Catalyst for Hydrolytic Dehydrogenation of Ammonia Borane. *J. Am. Chem. Soc.* **2010**, *132*, 5326–5327.
2. Zhang, K.; Xiang, Y.; Wu, X.; Feng, L.; He, W.; Liu, J.; Zhou, W.; Xie, S. Enhanced Optical Responses of Au@Pd Core/Shell Nanobars. *Langmuir* **2009**, *25*, 1162–1168.
3. Lu, C.; Prasad, K.; Wu, H.; Ho, J.; Huang, M. Au Nanocube-Directed Fabrication of Au–Pd Core–Shell Nanocrystals with Tetrahexahedral, Concave Octahedral, and Octahedral Structures and Their Electrocatalytic Activity. *J. Am. Chem. Soc.* **2010**, *132*, 14546–14553.
4. Tao, F.; Grass, M.; Zhang, Y.; Butcher, D.; Renzas, J.; Liu, Z.; Chung, J.; Mun, B.; Salmeron, M.; Somorjai, G. Reaction-Driven Restructuring of Rh–Pd and Pt–Pd Core–Shell Nanoparticles. *Science* **2008**, *322*, 932–934.
5. Ma, Y.; Li, W.; Cho, E.; Li, Z.; Yu, T.; Zeng, J.; Xie, Z.; Xia, Y. Au@Ag Core–Shell Nanocubes with Finely Tuned and Well-Controlled Sizes, Shell Thicknesses, and Optical Properties. *ACS Nano* **2010**, *4*, 6725–6734.
6. Lim, B.; Wang, J.; Camargo, P.; Jiang, M.; Kim, M.; Xia, Y. Facile Synthesis of Bimetallic Nanoplates Consisting of Pd Cores and Pt Shells through Seeded Epitaxial Growth. *Nano Lett.* **2008**, *8*, 2535–2540.
7. Wang, A.; Peng, Q.; Li, Y. Rod-Shaped Au–Pd Core–Shell Nanostructures. *Chem. Mater.* **2011**, *23*, 3217–3222.
8. Xia, Y.; Xiong, Y.; Lim, B.; Skrabalak, S. Shape-Controlled Synthesis of Metal Nanocrystals: Simple Chemistry Meets Complex Physics? *Angew. Chem., Int. Ed.* **2009**, *48*, 60–103.
9. Zhang, H.; Jin, M.; Wang, J.; Kim, M.; Yang, D.; Xia, Y. Nanocrystals Composed of Alternating Shells of Pd and Pt Can Be Obtained by Sequentially Adding Different Precursors. *J. Am. Chem. Soc.* **2011**, *133*, 10422–10425.
10. Wang, F.; Sun, L.; Feng, W.; Chen, H.; Yeung, M.; Wang, J.; Yan, C. Heteroepitaxial Growth of Core–Shell and Core–Multishell Nanocrystals Composed of Palladium and Gold. *Small* **2010**, *6*, 2566–2575.
11. Jiang, M.; Lim, B.; Tao, J.; Camargo, P.; Ma, C.; Zhu, Y.; Xia, Y. Epitaxial Overgrowth of Platinum on Palladium Nanocrystals. *Nanoscale* **2010**, *2*, 2406–2411.
12. Lim, B.; Kobayashi, H.; Yu, T.; Wang, J.; Kim, M.; Li, Z.; Rycenga, M.; Xia, Y. Synthesis of Pd–Au Bimetallic Nanocrystals *via* Controlled Overgrowth. *J. Am. Chem. Soc.* **2010**, *132*, 2506–2507.
13. Fan, F.; Liu, D.; Wu, Y.; Duan, S.; Xie, Z.; Jiang, Z.; Tian, Z. Epitaxial Growth of Heterogeneous Metal Nanocrystals: From Gold Nano-octahedra to Palladium and Silver Nanocubes. *J. Am. Chem. Soc.* **2008**, *130*, 6949–6951.
14. Habas, S.; Lee, H.; Radmilovic, V.; Somorjai, G.; Yang, P. Shaping Binary Metal Nanocrystals through Epitaxial Seeded Growth. *Nat. Mater.* **2007**, *6*, 692–697.
15. Lee, Y.; Kim, M.; Kim, Z.; Han, S. One-Step Synthesis of Au@Pd Core–Shell Nanooctahedron. *J. Am. Chem. Soc.* **2009**, *131*, 17036–17037.
16. Xiang, Y.; Wu, X.; Liu, D.; Jiang, X.; Chu, W.; Li, Z.; Ma, Y.; Zhou, W.; Xie, S. Formation of Rectangularly Shaped Pd/Au Bimetallic Nanorods: Evidence for Competing Growth of the Pd Shell between the {110} and {100} Side Facets of Au Nanorods. *Nano Lett.* **2006**, *6*, 2290–2294.
17. Sobal, N.; Ebels, U.; Mohwald, H.; Giersig, M. Synthesis of Core–Shell PtCo Nanocrystals. *J. Phys. Chem. B* **2003**, *107*, 7351–7354.
18. Yan, J.; Zhang, X.; Akita, T.; Haruta, M.; Xu, Q. One-Step Seeding Growth of Magnetically Recyclable Au@Co Core–Shell Nanoparticles: Highly Efficient Catalyst for Hydrolytic Dehydrogenation of Ammonia Borane. *J. Am. Chem. Soc.* **2010**, *132*, 5326–5327.

19. Sobal, N.; Hilgendorff, M.; Mohwald, H.; Giersig, M.; Spasova, M.; Radetic, T.; Farle, M. Synthesis and Structure of Colloidal Bimetallic Nanocrystals: The Non-Alloying System Ag/Co. *Nano Lett.* **2002**, *2*, 621–624.
20. Tsuji, M.; Yamaguchi, D.; Matsunaga, M.; Alam, M. Epitaxial Growth of Au@Cu Core–Shell Nanocrystals Prepared Using the PVP-Assisted Polyol Reduction Method. *Cryst. Growth Des.* **2010**, *10*, 5129–5135.
21. Tsuji, M.; Yamaguchi, D.; Matsunaga, M.; Ikedo, K. Epitaxial Growth of Au@Ni Core–Shell Nanocrystals Prepared Using a Two-Step Reduction Method. *Cryst. Growth Des.* **2011**, *11*, 1995–2005.
22. Zeng, J.; Zhu, C.; Tao, J.; Jin, M.; Zhang, H.; Li, Z.; Zhu, Y.; Xia, Y. Controlling the Nucleation and Growth of Silver on Palladium Nanocubes by Manipulating the Reaction Kinetics. *Angew. Chem., Int. Ed.* **2012**, in press (DOI: 10.1002/anie.201107061).
23. Jin, M.; He, G.; Zhang, H.; Zeng, J.; Xie, Z.; Xia, Y. Shape-Controlled Synthesis of Copper Nanocrystals in an Aqueous Solution with Glucose as a Reducing Agent and Hexadecylamine as a Capping Agent. *Angew. Chem., Int. Ed.* **2011**, *50*, 10560–10564.
24. Jin, M.; Liu, H.; Zhang, H.; Xie, Z.; Liu, J.; Xia, Y. Synthesis of Pd Nanocrystals Enclosed by {100} Facets and with Sizes <10 nm for Application in CO Oxidation. *Nano Res.* **2011**, *4*, 83–91.
25. Nikoobakht, B.; El-Sayed, M. Preparation and Growth Mechanism of Gold Nanorods (NRs) Using Seed-Mediated Growth Method. *Chem. Mater.* **2003**, *15*, 1957–1962.
26. Murphy, C.; Sau, T.; Gole, A.; Orendorff, C.; Gao, J.; Gou, L.; Hunyadi, S.; Li, T. Anisotropic Metal Nanoparticles: Synthesis, Assembly, and Optical Applications. *J. Phys. Chem. B* **2005**, *109*, 13857–13870.
27. Murphy, C.; Gole, A.; Hunyadi, S.; Orendorff, C. One-Dimensional Colloidal Gold and Silver Nanostructures. *Inorg. Chem.* **2006**, *45*, 7544–7554.
28. Jin, M.; Zhang, H.; Xie, Z.; Xia, Y. Palladium Concave Nanocubes with High-Index Facets and Their Enhanced Catalytic Properties. *Angew. Chem., Int. Ed.* **2011**, *50*, 7850–7854.
29. Grzelczak, M.; Rodriguez-Gonzalez, B.; Perez-Juste, J.; Liz-Marzan, L. Quasi-Epitaxial Growth of Ni Nanoshells on Au Nanorods. *Adv. Mater.* **2007**, *19*, 2262–2266.
30. Datta, K.; Kulkarni, C.; Eswaramoorthy, M. Aminoclay: A Permselective Matrix to Stabilize Copper Nanoparticles. *Chem. Commun.* **2010**, *46*, 616–618.
31. Datta, K.; Eswaramoorthy, M.; Rao, C. Water-Solubilized Aminoclay–Metal Nanoparticle Composites and Their Novel Properties. *J. Mater. Chem.* **2007**, *17*, 613–615.
32. Salzemann, C.; Brioude, A.; Pileni, M. Tuning of Copper Nanocrystals Optical Properties with Their Shapes. *J. Phys. Chem. B* **2006**, *110*, 7208–7212.
33. Wang, F.; Shen, Y. General Properties of Local Plasmons in Metal Nanostructures. *Phys. Rev. Lett.* **2006**, *97*, 206806.
34. Zhang, Q.; Li, W.; Moran, C.; Zeng, J.; Chen, J.; Wen, L.; Xia, Y. Seed-Mediated Synthesis of Ag Nanocubes with Controllable Edge Lengths in the Range of 30–200 nm and Comparison of Their Optical Properties. *J. Am. Chem. Soc.* **2010**, *132*, 11372–11378.
35. Jin, M.; Kuang, Q.; Han, X.; Xie, S.; Xie, Z.; Zheng, L. Liquid–Liquid Interface Assisted Synthesis of Size- and Thickness-Controlled Ag Nanoplates. *J. Solid State Chem.* **2010**, *183*, 1354–1358.
36. Murphy, C.; Sau, T.; Gole, A.; Orendorff, C. Surfactant-Directed Synthesis and Optical Properties of One-Dimensional Plasmonic Metallic Nanostructures. *MRS Bull.* **2005**, *30*, 349–355.
37. Niu, W.; Li, Z.; Shi, L.; Liu, X.; Li, H.; Han, S.; Chen, J.; Xu, G. Seed-Mediated Growth of Nearly Monodisperse Palladium Nanocubes with Controllable Sizes. *Cryst. Growth Des.* **2008**, *8*, 4440–4444.
38. Jin, M.; Zhang, H.; Xie, Z.; Xia, Y. Palladium Nanocrystals Enclosed by {100} and {111} Facets in Controlled Proportions and Their Catalytic Activities for Formic Acid Oxidation. *Energy Environ. Sci.* **2012**, in press (DOI: 10.1039/c2ee02866b).